
INHOMOGENEOUS ILLUMINATED IMAGE ENHANCEMENT UNDER EXTREMELY LOW VISIBILITY CONDITION

A PREPRINT

Libang Chen, Yikun Liu

School of Physics and Astronomy
Sun Yat-Sen University

Zhuhai 519082, China {Yikun_Liu}liuyk6@mail.sysu.edu.cn

Jianying Zhou

School of Physics
Sun Yat-Sen University
Guangzhou 510275

April 29, 2024

ABSTRACT

Imaging through fog significantly impacts fields such as object detection and recognition. In conditions of extremely low visibility, essential image information can be obscured, rendering standard extraction methods ineffective. Traditional digital processing techniques, such as histogram stretching, aim to mitigate fog effects by enhancing object light contrast diminished by atmospheric scattering. However, these methods often experience reduce effectiveness under inhomogeneous illumination. This paper introduces a novel approach that adaptively filters background illumination under extremely low visibility and preserve only the essential signal information. Additionally, we employ a visual optimization strategy based on image gradients to eliminate grayscale banding. Finally, the image is transformed to achieve high contrast and maintain fidelity to the original information through maximum histogram equalization. Our proposed method significantly enhances signal clarity in conditions of extremely low visibility and outperforms existing algorithms.

1 Introduction

In ideal scenarios, an optical imaging system achieves a point-to-point mapping between the object and the image, capturing pristine information. However, through the atmosphere, the optical transmission process is disturbed, resulting in poor imaging quality over long distances. During transmission, the inevitable processes including atmospheric absorption, resulting in low contrast of light, and atmospheric scattering, bringing noises to original light field, is considered irreversible and entropy gaining, due to the complexity [1, 2]. Under conditions of extremely low visibility, particularly when the imaging distance exceeds the Meteorological Optical Range, reconstructing images becomes challenging. Yet for civilian, military, and commercial uses, extending the imaging distance through atmospheric scattering media to collect the desired light information is vital.

Numerous methods have been developed to reconstruct information digitally under adverse weather conditions such as fog, haze, and sandstorms [3, 4, 5, 6, 7, 8]. The common idea across these methods is to suppress the scattered light and to recover information by utilizing the ballistic light, which contains the un-scattered information through the atmosphere. The comprehensive way is to amplify the captured image by a reasonable mapping, maintaining the fidelity while increasing its contrast, thus to enhance the perceptibility of a system. Amongst, Histogram equalization (HE) is proven an efficient way of mapping [9], utilizing the image's cumulative density function (CDF) to enhance visual contrast. The evolution of HE follows Contrast Clipped Adaptive histogram equalization (CLAHE) [10, 11], which includes dividing image into fractions for localized HE and applying a bilinear interpolation between the boundaries of the blocks. Based on CLAHE, the following algorithms were proposed [12, 13, 14]. Though being quite successful to tackle the majority of scenarios pertaining atmospheric scattering, under scenarios such as inhomogeneous illuminations, the discontinuity of image blocks can sabotage image quality.

Generally, the inhomogeneity of illumination roots from the vignetting effects of the lenses, inconformity of the camera pixel response, and the inhomogeneity of illumination. Traditional illumination inhomogeneity correction of the image is by computing the difference between spatially placed illumination and the acquired image illumination. In digital

processing, methods such as top-hat transformation [15] and low-rank and sparse decomposition [16] achieve good effects in general, however preserving details of the image for a single image input is still a challenge. The single scale retinex (SSR) [17, 18] and multi scale retinex (MSR) [19] use Gaussian kernel to filter the image. However, the methods require a manual selection of filter parameters, and the enhancement is normally a linear stretching or exponential transformation. In extremely low visibility, the reconstructing effects is not sufficient.

Inspired by literature [11, 17, 19], this paper proposes an enhancement technic called Homogeneous Maximum Histogram Equalization (HMHE). We propose an empirical method to evaluate the image information's residuality, thus automatically select the appropriate filtering kernel and remove the inhomogeneous illumination. In the meantime, the grayscale banding effects brought by filtering is removed by a visual optimization algorithm based on the image gradient. Ultimately, the filtered image is enhanced through the proposed Maximum Histogram Equalization (MHE), which scales the regular HE to maximize its ability to enhance images. Experiments have discovered that the proposed method can fully utilize the ballistic signals with high fidelity through scattering media, bringing the highest contrast of desired targets. The results can be a good image preprocessing methods for deeper usage in applying neural network to further process the image.

The paper is arranged as follows: In section 2, we will briefly introduce the physical models in atmospheric imaging and the fundamental idea of the filtering algorithm and visual optimization algorithm. In section 3, several conventional image enhancement algorithms are compared, with qualitative results and discussion of the differences. The conclusion will be given in section 4.

2 The theory

2.1 Low visibility imaging model

The optical process through scattering media is described by [20, 21]. Due to the scattering effects, the reflected light from object is divided into the ballistic light, the snake light, which is slightly scattered, forming the noise component of the passing light, and the scattered light, which suffers multiple scattering, and becomes a global interference and noise. Therefore, we can write:

$$I_{view} = I_{obj}T + I_{sna} + I_{sca} = I_{obj}T + I_{sna} + I_{illu}(1 - T) \quad (1)$$

Where I_{view} , I_{obj} , I_{sna} , I_{sca} , and I_{illu} are the viewed light, the reflected light from object, the snake light, the scattered light, and the ambient illumination. The ballistic light follows geometric optics, and suffers degradation by the lambert-beer law as $T = \exp(-\beta_{ext}L)$. β_{ext} and L are the extinction coefficient and distance respectively. Thus, I_{view} has the property of low contrast and low signal-to-noise ratio.

2.2 inhomogeneity correction

We denote the imaged intensity with inhomogeneous illumination as the simple sum of the below quantities [22]:

$$N(x, y) = U(x, y) + A(x, y) + N(x, y) \quad (2)$$

Where $U(x, y)$, $A(x, y)$, and $N(x, y)$ are the image of the object, the illumination, and the additive noise. x, y are the transverse and vertical positions. We assume the illumination is of low frequency term [16], and the desired target at a distance is of high frequency. By applying an appropriate low pass filter (LPF), we'll achieve the low frequency components of the total intensity:

$$N_{LPF}(x, y) = A(x, y) + U_{low}(x, y) \quad (3)$$

Where $U_{low}(x, y)$ is the low frequency parts of the object information. Thus, the image with only the useful information can be expressed as:

$$N_{homogeneous}(x, y) = N(x, y) - N_{LPF}(x, y) \quad (4)$$

The transformation from light to digits is denoted as f . In expression of the light field:

$$N_{homogeneous}(x, y) = f \left[I_{obj}^{high}T + I_{sna} \right] \quad (5)$$

By enhancing the homogeneous components of the original image, the interference of the illumination is eliminated.

2.3 Maximum histogram equalization

HE is a simple image enhancement algorithm to enhance the original contrast by means of projecting intensity by the CDF [23]. Assuming the allowed discrete value $\mathbb{Z} \in [0, L - 1]$, where L is the maximum grayscale of the camera. The histogram of an image is $H(i) = n(i)/MN$, where i represents one of the values in \mathbb{Z} , and $H(i)$ represents the number of pixels which has the intensity i . M, N are the number of pixels in vertical and horizontal direction respectively. The CDF of is denoted as $D(i) = \sum_{k=0}^i H(k)/MN$. We denote the enhanced intensity as e . We propose the maximum histogram equalization (MHE) by the above equation:

$$e = (L - 1) [D(i) - D(i_{min})] / (D(i_{max}) - D(i_{min})) \quad (6)$$

The enhancement technic effectively amplifies the original signal with high fidelity by keeping the original signal value relationship following the CDF.

2.4 Contrast of the enhanced image

The contrast of an object is defined as:

$$C = \frac{i_{bright} - i_{dark}}{i_{bright} + i_{dark}} \quad (7)$$

We denote the histogram of the inhomogeneous illuminated image as $H'(i)$, The object and background intensity are i_{bright} and i_{dark} respectively. The illumination corrected histogram is $H(i)$. We then compare the contrast of the HE (C_{HE}) and HMHE (C_{HMHE}) enhanced contaminated image:

$$C_{HE} = \frac{\sum_{k=0}^{i_{bright}} H'(k) - \sum_{k=0}^{i_{dark}} H'(k)}{\sum_{k=0}^{i_{bright}} H'(k) + \sum_{k=0}^{i_{dark}} H'(k)} \quad (8)$$

$$C_{HMHE} = \frac{\sum_{k=0}^{i_{bright}} H(k) - \sum_{k=0}^{i_{dark}} H(k)}{\sum_{k=0}^{i_{bright}} H(k) + \sum_{k=0}^{i_{dark}} H(k) - 2H(i_{min})} \quad (9)$$

It can be seen for Eq.(8), (9) that the contrast of the HMHE enhanced image incorporates a negative term in the denominator, thus compared to the HE enhanced image, assuming identical histograms for both, the amplification of contrast is significant. Fig. 1 (a), (b), (c), and (d) demonstrates the original and enhanced histogram of the contaminated image, original and enhanced histogram of the uncontaminated image respectively. Owing to the illumination, the histogram is inevitably widened, leading to a weakened enhancement space for signal, and an unwanted enhancement of the illumination, leading to poor image quality.

3 The algorithm

3.1 Overview

The HMHE consists of 3 parts. The background light extraction, the visual enhancement, and the image enhancement. In the background light extraction module, an estimator based on structure similarity index measurement (SSIM) [24] is proposed to assure the filtering of only the background light, remaining the desired signals. In the visual perception optimization module, it addresses the grayscale banding introduced due to applying a LPF to the image. In the image enhancement module, it stretches the overall image histogram. In the end, the mean filtering is applied to generate the final the image output.

3.2 Inhomogeneous illumination estimation

For images corrupted by inhomogeneous illumination, estimating the background light is crucial. Since inhomogeneous illumination is typically a low-frequency signal, we can use a low-pass filter to estimate and remove the background light. However, for complex scenes, the selection of filter parameters is critical. An adaptive algorithm based

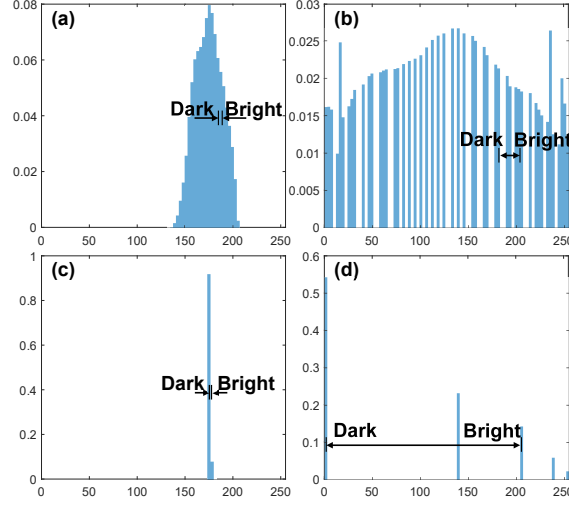


Figure 1: An illustration of histogram for different images. (a) histogram in low visibility condition with incongruent light. (b) original histogram. (c) HE for (a). (d) MHE for (b).

on image features to automatically estimate the appropriate filter size, effectively removing non-uniform illumination while preserving image details is proposed.

The background light estimation principle is low-pass filtering. We perform a 2D fast Fourier transform on the image, then multiply the low-pass filter spectrum with the image spectrum. We obtain the low-frequency image by taking the inverse Fourier transform. This process is similar to homomorphic filtering [25]. To prevent negative values, we add the original image's mean to the filtered image.

$$I_{filtered}(x, y) = I_{congruent}(x, y) + \overline{I(x, y)} \quad (10)$$

We can write the SSIM of the original image and the filtered image:

$$SSIM(X, Y) = \frac{2\mu_X\mu_Y(2\sigma_{XY} + C_2)}{(\mu_X^2 + \mu_Y^2 + C_1)(\sigma_X^2 + \sigma_Y^2 + C_2)} \quad (11)$$

Where X , Y are the original and filtered image, σ_x and σ_y are the variances, σ_{xy} is the covariance, $C_1 = (K_1L)^2$, $C_2 = (K_2L)^2$ are the regulation constants, K_1 , K_2 are two small constants. SSIM has sufficient resolution to judge the similarity between two images. In our study, the criteria for determining if the low-pass filter cutoff kernel k_{cutoff} is sufficiently large is given by the absolute of the first and second derivatives of the SSIM over kernel size as the following expression:

$$k_{cutoff} = \max \left\{ \argmin_k \left| \frac{\partial^i SSIM(X, Y_{[k]})}{\partial [k]^i} \right| \right\}, \text{ for } i = 1, 2 \quad (12)$$

Where ∂ is the differential operator, $[\cdot]$, and $|\cdot|$ denotes taking the integer and the absolute value of the variable. These derivatives are instrumental when adjusting the low-pass filter's cutoff kernel to evaluate the impact on image quality. Initially, as the kernel begins to exclude the image's effective information, SSIM experiences a notable decrease, indicating the loss of essential details. This stage highlights the importance of the derivatives: the first derivative captures how swiftly structural similarity diminishes, while the second derivative identifies critical points where this rate of change shifts. Once the filter removes all effective information, further enlarging the kernel impacts SSIM minimally, as the remaining low-frequency components do not significantly affect the image's structural similarity. The optimal balance between eliminating irrelevant noise and preserving vital structural features is achieved by applying the minimum absolute values of the two derivatives, ensuring the selected cutoff kernel maintains image quality by keeping significant structural information intact.

Fig. 2 (a), (b), (c) demonstrates a high information scenario of the original, filtered with our algorithm and its SSIM relationship with the kernel respectively along with Fig. 2 (d), (e), (f), a low information scenario. In the first scenario, the useful information consists mainly of high frequency, thus the resulted kernel size is 48, while the second scenario, where the target consists of two floaters in the ocean, consisting of lower frequency, acquires a larger kernel size of 128 to fully filter the information.

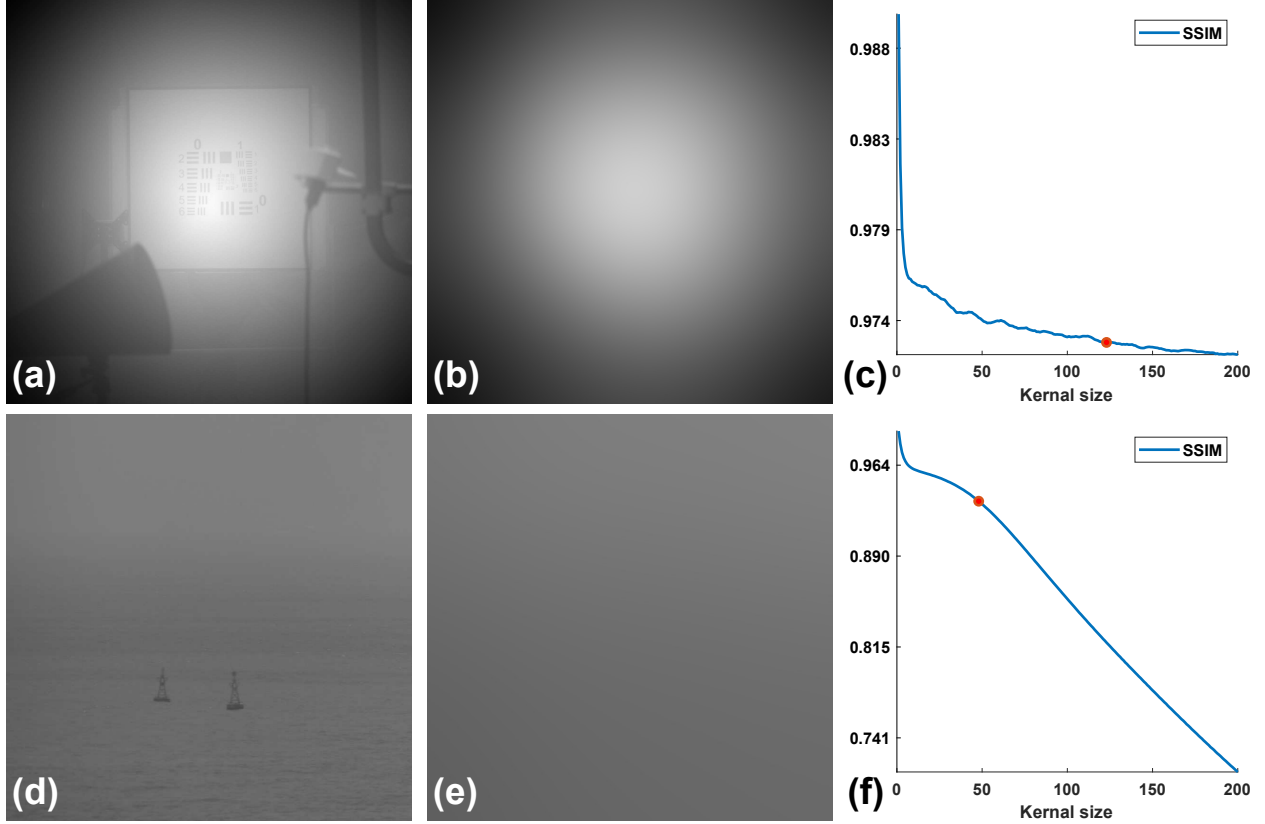


Figure 2: A demonstration of the illumination estimation algorithm. (a), (d) original image, (b), (e) filtered image, and (c), (f) the SSIM relation with the kernel size.

3.3 Visual optimization

A direct application of low-pass filtering to an image results in the grayscale banding effect. If this phenomenon is not addressed, the final enhanced image will have a poor visual perception. The reason for this effect is that the low-frequency components of the image decrease in a stair-stepping manner in the spatial domain, leading to images similar to contours. Moreover, when performing global mapping, these bandings will be amplified, creating disturbed image. We eliminate the artefacts by adding an interference to the bands:

$$I_{filtered}^{visual}(x, y) = I_{filtered}(x + m, y + n) + n(x + m, y + n) \quad (13)$$

Where $I_{filtered}^{visual}$ is the optimized image. n is the added gaussian noise whose standard variance satisfies $\sigma(n) = \max[gradient(I_{filtered})]/3$. The comparison between the image before and after the visual optimization algorithm are shown in Fig. 3, where Fig. 3 (a)-(d) demonstrates the original filtered images whereas Fig. 3 (e)-(h) are the filtered images after the visual optimization algorithm. Specifically, Fig. 3(a), (d) are the processing results in the fog chamber, while Fig. 3 (b), (c) are outdoor natural low-visibility scenes. It can be seen from the results that the banding effect is visually resolved after applying the visual optimization algorithm.

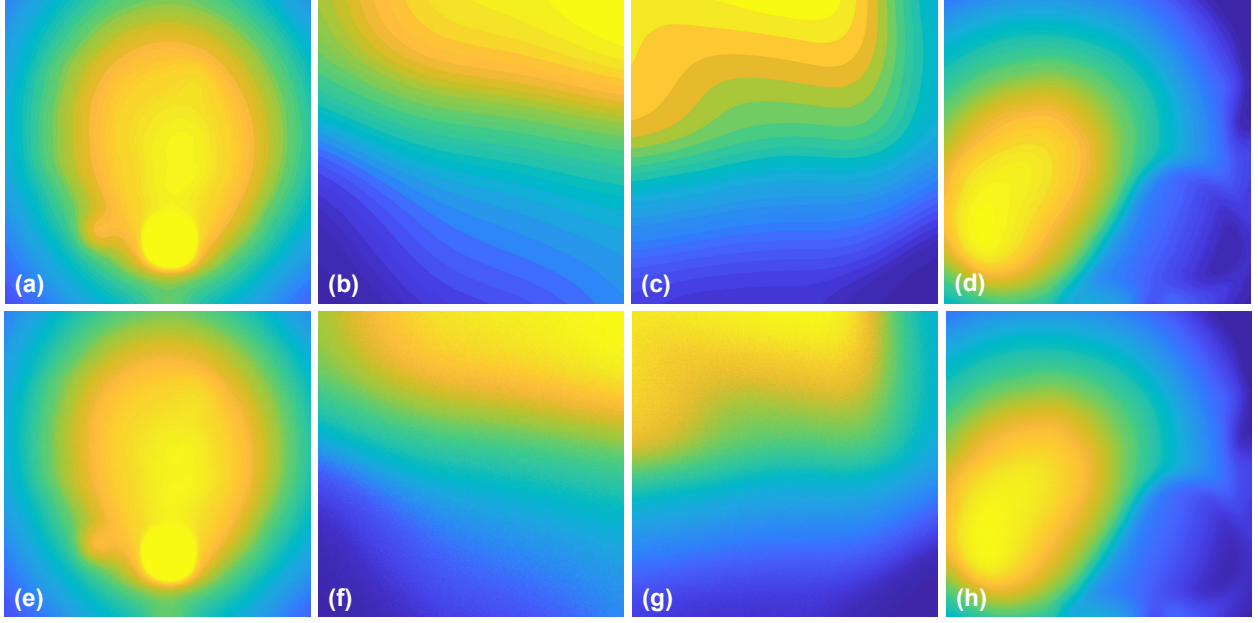


Figure 3: Comparison of filtered image before visual optimization algorithm (a)-(d) and after (e)-(h) in different scenarios.

3.4 Image enhancement

The image enhancement algorithm used is mentioned in section 2.3. The HMHE is an improved HE. When images are filtered by a large kernel, they demonstrate a dense distribution in the histogram, leading regular HE unable to amplify the image. By linear stretching the post-enhanced image, the HMHE reaches the maximum available contrast of the original image following the rules of HE, leading to high contrast while preserving image fidelity.

4 Experimental results and discussion

4.1 Experiment

To thoroughly verify the effectiveness of the algorithm proposed in this paper, experiments were conducted in both indoor and outdoor settings. Thus, our data encompasses scenarios involving indoor lighting and artificial fog, as well as natural sunlight and natural fog. To rigorously assess the robustness of the algorithm, experiments were carried out using cameras and lenses of various models. The cameras used in the experiments include the Basler acA3088-57um, PCO EDGE 4.2, and Hamamatsu C11440-22CU, with resolutions of 3088x2064 pixels, 8-bit depth; 2048x2048 pixels, 16-bit depth; and 2048x2048 pixels, 16-bit depth, respectively. The lenses employed were the Computar M7528-MP and the Zeiss Milvus 2/100M.

The indoor experiments were conducted at the Visibility Calibration Laboratory of the China Meteorological Administration in Shanghai, China. We used targets of varying spatial frequencies, shapes, and distances to mimic real-world natural scenes. Due to the controllable fog density in the indoor fog chamber, we were able to obtain clear images without fog, which offers a significant advantage for evaluating the algorithm. The data from outdoor experiments were used to further validate the reliability of the algorithm.

4.2 Evaluation metrics

For quantitative evaluation, we selected the following Image Quality Assessment (IQA) metrics:

Average Local Contrast (ALC) [26] is defined as:

$$ALC = \frac{1}{GF} \sum_i \frac{\sigma_i^2}{\mu_i + c} \quad (14)$$

Where, σ_i^2 , μ_i represents the variance and the mean of the i -th block of the image respectively, and c is a small constant set to 0.0001. The block is a sliding 100×100 window w . The image is divided into $G \times F$ blocks by the window.

Mean Measure of Enhancement [27] (MEME) is highly related to image contrast, defined as the mean of EME:

$$EME = \frac{1}{w^2} \sum_{k=1}^w \sum_{l=1}^w 20 \log_{10} \left(\frac{I_{max;k,l}}{I_{min;k,l} + c} \right) \quad (15)$$

Where $I_{max;k,l}$ and $I_{min;k,l}$ are the maximum and minimum values within a local image region, respectively.

Information entropy (IE) evaluates the average entropy of an image. A lower entropy indicates higher image purity and distinct structure [28]. The definition of IE for any given image is:

$$IE = - \sum p_i \log_2 p_i \quad (16)$$

Where p_i is the probability of a particular gray level in the image.

Similar to MEME, MAME [29] is a contrast calculation method based on contrast entropy, where AME is expressed as:

$$AME = \frac{1}{w^2} \sum_{k=1}^w \sum_{l=1}^w 20 \ln \left(\frac{I_{max;k,l} - I_{min;k,l}}{I_{max;k,l} + I_{min;k,l} + c} \right) \quad (17)$$

This definition directly calculates the contrast in a small area. Therefore, the closer AME is to 0, the greater the local contrast.

4.3 Comparisons with other image enhancement methods

In this paper, we compare the proposed algorithm with traditional low-visibility image enhancement algorithms, including HE, CLAHE [30], Dark Channel Prior (DCP) [31], and SSR. For the CLAHE algorithm, the clip limit for normalized images is set to 0.02, with image segmentation into 8×8 blocks. The DCP uses a per-channel patch size of 15×15 pixels. The SSR algorithm's low-pass filter standard deviation is set to 50 pixels. The experimental data from the fog chamber and the comparison results are illustrated in Fig. 4. Fig. 4 (a)-(c) depict three targets inside the fog chamber, where the leftmost column shows data captured in clear conditions. The second to seventh columns respectively showcase the original image, the outcomes of HE, CLAHE, DCP, SSR, and the algorithm proposed in this paper.

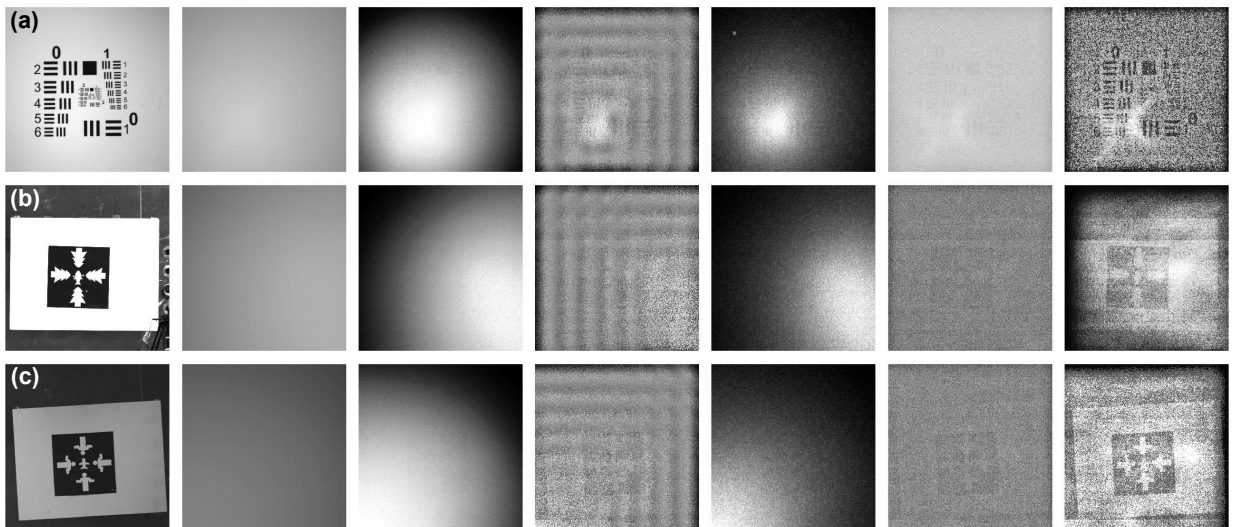


Figure 4: Visual comparison of image enhancement results using various algorithms on three distinct scenarios in the fog chamber (a) resolution test chart, (b) botanical pattern, and (c) group and aircraft pattern.

Table 1: ALC, MEME, IE, MAME values in the fog chamber

Figure	IQA	HE	CLAHE	DCP	SSR	Ours
4(a)	ALC	0.0050	0.0247	0.0131	0.0020	0.1254
	MEME	0.0034	0.0059	0.0094	0.0014	0.0313
	IE	5.7076	7.2508	7.4920	5.6232	1.3963
	MAME	-0.0107	-0.0042	-0.0032	-0.0139	-0.0001
4(b)	ALC	0.0022	0.0314	0.0105	0.0192	0.0512
	MEME	0.0024	0.0071	0.0077	0.0059	0.0085
	IE	5.7792	7.3805	7.0686	6.7467	2.1784
	MAME	-0.0120	-0.0035	-0.0042	-0.0032	-0.0027
4(c)	ALC	0.0021	0.0302	0.0116	0.0208	0.1178
	MEME	0.0022	0.0068	0.0079	0.0060	0.0120
	IE	5.6231	7.3399	7.566	6.8341	1.3693
	MAME	-0.0129	-0.0033	-0.0036	-0.0030	-0.0015

The data comparison reveals that, in indoor settings with severe uneven lighting, HE amplifies the uneven lighting interference while boosting the signal. CLAHE, due to significant differences in light intensity between blocks, faces difficulty in seamlessly integrating the light intensity of each tile, leading to noticeable block artifacts. Since indoor scenes lack consistent ambient light, DCP’s estimation deviates significantly from the actual attenuation model, rendering the per-channel image and ambient light estimation ineffective for image recovery. SSR, considering homomorphic filtering, successfully restores image information, but the restored contrast is low, making the signal difficult to observe clearly. Among the algorithms discussed, the one proposed in this paper achieves the best local contrast and image uniformity.

Quantitative evaluations corresponding to Fig. 4 are presented in Table 1, where the best scores are high-lighted with bold text. In assessing contrast metrics such as ALC, EME, AME, the algorithm proposed in this work consistently achieves better scores across the majority of scenarios, indicative of superior local contrast enhancement. Furthermore, regarding the IE metric, our algorithm invariably registers the lowest values, signifying the highest degree of image purity achieved.

The comparative analysis of experimental data from outdoor settings is depicted in Fig. 5. Figures 5(a)-(c) showcase three distinct outdoor scenarios. Sequentially from left to right, each set presents the original images followed by the results processed through HE, CLAHE, DCP, SSR, and the algorithm proposed herein. Analogous to indoor findings, HE’s performance in outdoor environments mirrors its indoor application. The restoration quality of CLAHE sees substantial improvement due to the diminished irregularities in lighting, resulting in nearly imperceptible block effects and the preservation of image details. Given that outdoor scenes more closely align with the atmospheric attenuation model, DCP demonstrates enhanced visual outcomes compared to indoor applications. Despite SSR’s capacity to restore images, it continues to yield comparatively lower contrast. Notably, the proposed algorithm successfully recovers critical visual elements such as the houses in Fig. 5(a), the road in Fig. 5(b), and the houses in Fig.5(c) within outdoor scenes. Quantitative assessments are shown in Table 2, where the best scores are high-lighted with bold text.

Table 2: ALC, MEME, IE, MAME values in outdoor scenes

Figure	IQA	HE	CLAHE	DCP	SSR	Ours
5(a)	ALC	0.0101	0.0767	0.0214	0.0052	0.1257
	MEME	0.0012	0.0034	0.0024	0.0013	0.0057
	IE	5.2562	7.8875	7.7626	4.9278	3.3111
	MAME	-0.0017	-0.0002	-0.0007	-0.001	-0.0001
5(b)	ALC	0.0041	0.0502	0.0127	0.0050	0.1039
	MEME	0.0008	0.0027	0.0020	0.0009	0.0041
	IE	5.5833	7.7384	7.7935	5.4353	3.0602
	MAME	-0.0025	-0.0005	-0.0010	-0.0016	-0.0003
5(c)	ALC	0.0037	0.0330	0.0196	0.0198	0.0924
	MEME	0.0008	0.0021	0.0027	0.0018	0.0042
	IE	5.7560	7.4452	7.2804	6.6999	2.1950
	MAME	-0.0024	-0.0006	-0.0006	-0.0005	-0.0002

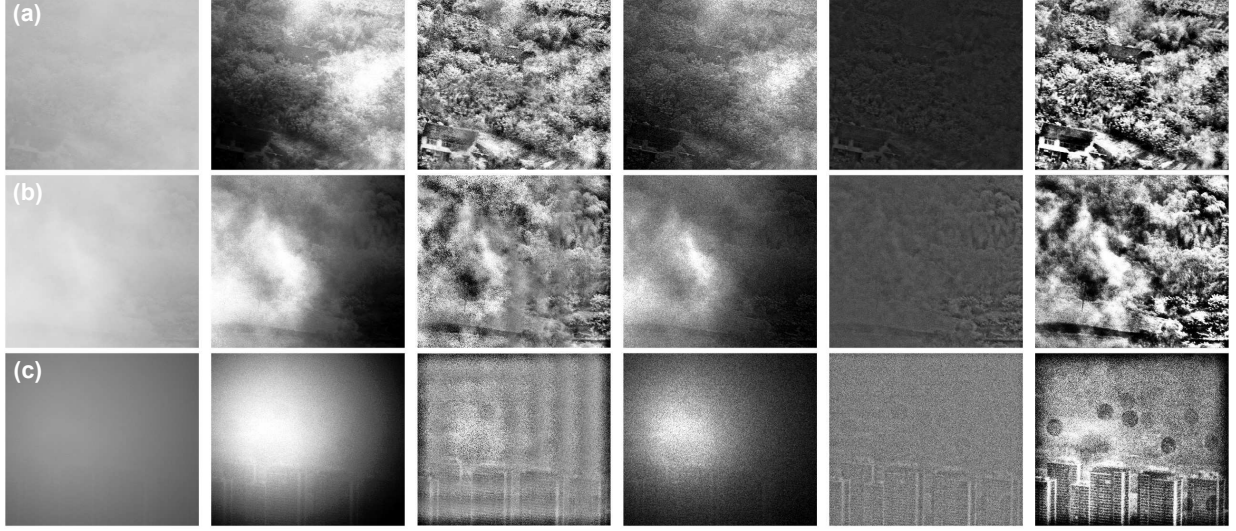


Figure 5: Visual comparison of image enhancement results using various algorithms across outdoor environments. (a) a house in a forest, (b) a road through a wooded area, and (c) an urban cityscape.

5 Conclusion

This study introduces a novel algorithm designed to substantially enhance image contrast under conditions of extremely low visibility. The algorithm strategically eliminates redundant information through a filtering process before proceeding to image enhancement. Given that scattered light, predominating under low visibility conditions, typically introduces low-frequency component disturbances, our method efficiently excises this redundant information. The appropriateness of a filter is adjudicated based on the structural similarity between the post-filtered and original images, with images deemed devoid of valuable information upon a significant shift in similarity rates. Post-filtering, images may exhibit a grayscale banding effect, which is effectively mitigated through deliberate disturbance introduction, thus ensuring an improved visual presentation. The algorithm concludes with a comprehensive global enhancement of the image. Through rigorous indoor and outdoor experimental validation, the algorithm has demonstrated a pronounced capability to enhance image contrast significantly, thereby maximizing the visibility of objects under severely limited visibility conditions.

Funding This work was supported by the Guangdong Major Project of Basic and Applied Basic Research (2020B0301030009); the National Natural Science Foundation of China (61991452, 12074444); and the National Key Research and Development Program of China (2022YFA1404300, 2020YFC2007102).

Disclosures The authors declare no conflicts of interest.

Data availability Data underlying the results presented in this paper are not publicly available at this time but may be obtained from the authors upon reasonable request.

References

- [1] Jacopo Bertolotti and Ori Katz. Imaging in complex media. *Nature Physics*, 18:1008 – 1017, 2022.
- [2] C. Brosseau and Dominique Bicot. Entropy production in multiple scattering of light by a spatially random medium. *Physical review. E, Statistical physics, plasmas, fluids, and related interdisciplinary topics*, 50:4997–5005, 01 1995.
- [3] Hui Cao, Allard Pieter Mosk, and Stefan Rotter. Shaping the propagation of light in complex media. *Nature Physics*, 18:994 – 1007, 2022.
- [4] Derya Akkaynak and Tali Treibitz. Sea-thru: A method for removing water from underwater images. *2019 IEEE/CVF Conference on Computer Vision and Pattern Recognition (CVPR)*, pages 1682–1691, 2019.
- [5] K. Sudhanthira and P. D. Sathya. Color balance and fusion for underwater image enhancement. 2019.

-
- [6] Zihong Chen, Liangyan Wang, Chunling Wang, and Yang Zheng. Fog image enhancement algorithm based on improved retinex algorithm. In *2022 3rd International Conference on Electronic Communication and Artificial Intelligence (IWECAI)*, pages 196–199, 2022.
 - [7] Ravinder Kaur and Mamta Juneja. A hybrid approach for enhancement of abdominal ct images. *Computers and Electrical Engineering*, 2022.
 - [8] Yunliang Qi, Zhen Yang, Wenhao Sun, Meng Lou, Jing Lian, Wenwei Zhao, Xiangyu Deng, and Yide Ma. A comprehensive overview of image enhancement techniques. *Archives of Computational Methods in Engineering*, 29:583 – 607, 2021.
 - [9] Nungsanginla Longkumer, Mukesh Kumar, and Rohini Saxena. Contrast enhancement techniques using histogram equalization: A survey. 2014.
 - [10] David J. Ketcham. Real-time image enhancement techniques. In *Other Conferences*, 1976.
 - [11] Stephen M. Pizer, E. Philip Amburn, John D. Austin, Robert Cromartie, Ari Geselowitz, Trey Greer, Bart ter Haar Romeny, John B. Zimmerman, and Karel Zuiderveld. Adaptive histogram equalization and its variations. *Computer Vision, Graphics, and Image Processing*, 39(3):355–368, 1987.
 - [12] Muhammad Suzuri Hitam, Wan Nural Jawahir Hj Wan Yussof, Ezmahamrul Afreen Awalludin, and Zainudin Bachok. Mixture contrast limited adaptive histogram equalization for underwater image enhancement. *2013 International Conference on Computer Applications Technology (ICCAT)*, pages 1–5, 2013.
 - [13] Anuradha Anuradha and Harsimranjeet Kaur. Enriched enhancement of underwater images by l^*a^*b on clahe and gradient based smoothing. *International Journal of Computer Applications*, 109:24–28, 2015.
 - [14] Umut Kuran and Emre Can Kuran. Parameter selection for clahe using multi-objective cuckoo search algorithm for image contrast enhancement. *Intell. Syst. Appl.*, 12:200051, 2021.
 - [15] Lizhen Deng, Jieke Zhang, Guoxia Xu, and Hu Zhu. Infrared small target detection via adaptive m-estimator ring top-hat transformation. *Pattern Recognit.*, 112:107729, 2020.
 - [16] Tingying Peng, Kurt S. Thorn, Timm Schroeder, Lichao Wang, Fabian J Theis, Carsten Marr, and Nassir Navab. A basic tool for background and shading correction of optical microscopy images. *Nature Communications*, 8, 2017.
 - [17] Daniel J. Jobson, Zia ur Rahman, and Glenn A. Woodell. Properties and performance of a center/surround retinex. *IEEE transactions on image processing : a publication of the IEEE Signal Processing Society*, 6 3:451–62, 1997.
 - [18] Mark S. Cohen, Richard M. DuBois, and Michael M. Zeineh. Rapid and effective correction of rf inhomogeneity for high field magnetic resonance imaging. *Human Brain Mapping*, 10, 2000.
 - [19] Zia ur Rahman, Daniel J. Jobson, and Glenn A. Woodell. Multi-scale retinex for color image enhancement. *Proceedings of 3rd IEEE International Conference on Image Processing*, 3:1003–1006 vol.3, 1996.
 - [20] Seibert Q. Duntley. The reduction of apparent contrast by the atmosphere. *J. Opt. Soc. Am.*, 38(2):179–191, Feb 1948.
 - [21] Robert R. Alfano, Wubao B. Wang, Leming Wang, and Swapan Kumar Gayen. Light propagation in highly scattering turbid media: Concepts, techniques, and biomedical applications. *Photonics*, pages 367–412, 2015.
 - [22] Bostjan Likar, J. B. Antoine Maintz, Max A. Viergever, and Franjo Pernus. Retrospective shading correction based on entropy minimization. *Journal of Microscopy*, 197, 2000.
 - [23] Rafael Corsino González, Richard E. Woods, and Barry R. Masters. Digital image processing, third edition. *Journal of Biomedical Optics*, 14:029901, 2009.
 - [24] Zhou Wang, Alan Conrad Bovik, Hamid R. Sheikh, and Eero P. Simoncelli. Image quality assessment: from error visibility to structural similarity. *IEEE Transactions on Image Processing*, 13:600–612, 2004.
 - [25] Yingbo Wang, Jie Cao, Saad Rizvi, Qun Hao, and Yami Fang. Underwater image restoration based on adaptive color compensation and dual transmission estimation. *IEEE Access*, 8:207834–207843, 2020.
 - [26] Eli Peli. Contrast in complex images. *Journal of the Optical Society of America. A, Optics and image science*, 7 10:2032–40, 1990.
 - [27] Sos S. Agaian, Karen Panetta Lentz, and Artyom M. Grigoryan. A new measure of image enhancement. 2000.
 - [28] Julio César Mello Román, José Luis Vázquez Noguera, Horacio Legal-Ayala, Diego P. Pinto-Roa, Santiago Gomez-Guerrero, and Miguel García Torres. Entropy and contrast enhancement of infrared thermal images using the multiscale top-hat transform. *Entropy*, 21(3), 2019.

- [29] Sos S. Aghaian, Blair Silver, and Karen A. Panetta. Transform coefficient histogram-based image enhancement algorithms using contrast entropy. *IEEE Transactions on Image Processing*, 16(3):741–758, 2007.
- [30] Karel J. Zuiderveld. Contrast limited adaptive histogram equalization. In *Graphics gems*, 1994.
- [31] Kaiming He, Jian Sun, and Xiaoou Tang. Single image haze removal using dark channel prior. *2009 IEEE Conference on Computer Vision and Pattern Recognition*, pages 1956–1963, 2009.